Numerical simulation of the neutral equilibrium atmospheric boundary layer using the SST *k-ω* turbulence model

Peng Hu[1], Yongle Li[*1], C.S. Cai[2], Haili Liao[1] and G.J. Xu[2]

[1]*Department of Bridge Engineering, Southwest Jiaotong University, Chengdu, Sichuan 610031, China*
[2]*Department of Civil and Environmental Engineering, Louisiana State University, Baton Rouge, Louisiana 70803, USA*

Abstract. Modeling an equilibrium atmospheric boundary layer (ABL) in an empty computational domain has routinely been performed with the *k-ε* turbulence model. However, the research objects of structural wind engineering are bluff bodies, and the SST *k-ω* turbulence model is more widely used in the numerical simulation of flow around bluff bodies than the *k-ε* turbulence model. Therefore, to simulate an equilibrium ABL based on the SST *k-ω* turbulence model, the inlet profiles of the mean wind speed U, turbulence kinetic energy k, and specific dissipation rate ω are proposed, and the source terms for the U, k and ω are derived by satisfying their corresponding transport equations. Based on the proposed inlet profiles, numerical comparative studies with and without considering the source terms are carried out in an empty computational domain, and an actual numerical simulation with a trapezoidal hill is further conducted. It shows that when the source terms are considered, the profiles of U, k and ω are all maintained well along the empty computational domain and the accuracy of the actual numerical simulation is greatly improved. The present study could provide a new methodology for modeling the equilibrium ABL problem and for further CFD simulations with practical value.

Keywords: equilibrium atmospheric boundary layer; SST *k-ω* turbulence model; source terms; inlet profiles; Computational Fluid Dynamic (CFD)

1. Introduction

With the development of numerical solution methods and computer hardware, the application of Computational Fluid Dynamics (CFD) in structural wind engineering has become an important subject for study. Generally speaking, the bodies of interest in structural wind engineering are bluff bodies, and they are in the lower part of the atmospheric boundary layer (ABL). Since the ABL flow around bluff structure bodies could be very complicated, to accurately simulate the complex flow in the computational domain, it is imperative to obtain accurate and reliable predictions of wind loads on structures. However, an equilibrium ABL (or horizontal homogeneity ABL) should be modeled first in an empty computational domain before the actual CFD simulation, which means that the inlet profiles of the mean wind speed and turbulence properties should be maintained throughout the empty computational domain before the actual simulation with the

---

∗Corresponding author, Professor, E-mail: lele@swjtu.edu.cn

structure model.

Achieving an equilibrium ABL is an important precondition for the actual CFD simulation, since a non-equilibrium ABL may result in significant errors. Blocken *et al.* (2007a) studied the wind speed conditions at the pedestrian height along the passage centre line between two parallel buildings, and found a systematic 15% discrepancy exists between the computation results and the corresponding measurement data. They mentioned that the reason was that the inlet profile of the mean wind speed was not maintained along the computational domain, which caused the CFD reference incident wind speed to change. However, a very close agreement between the computation and measurement results was indeed obtained with the reference incident wind speed being corrected. In fact, many studies have emphasized the requirement of achieving an equilibrium ABL before an actual CFD simulation is carried out (Riddle *et al.* 2004, Franke *et al.* 2007, Blocken *et al.* 2007b, Yang *et al.* 2008, Gorlé *et al.* 2009, Parente *et al.* 2011, Blocken *et al.* 2012). Strictly speaking, an equilibrium ABL can only be obtained if the inlet profiles of the mean wind speed and turbulence properties are consistent with the turbulence model, the wall function, and the roughness modification (Blocken *et al.* 2007b).

Richards and Hoxey (1993) made some assumptions about the ABL and produced a suitable set of boundary conditions for the k-ε turbulence model to ensure an equilibrium ABL. However, Hargreaves and Wright (2007) pointed out that the boundary conditions of Richards and Hoxey (1993) were not sufficient to produce an equilibrium ABL when using the k-ε turbulence model in commercial CFD software, but with a modified wall function and with a shear stress applied to the top boundary of the computational domain, the ABL could be maintained along the length of fetch. Recently, Richards and Norris (2011) provided the inlet profiles and boundary conditions appropriate for modeling the equilibrium ABL flow using different RANS turbulence models by directly solving their transport equations. They found that the effective von Kármán constant depends on the other turbulence model constants. It should be pointed out that the above methods to model the equilibrium ABL are based on the constant turbulence kinetic energy k over the full height of ABL, which may not agree with the profiles measured in the atmosphere or generated in a wind tunnel.

Yang *et al.* (2009) proposed an alternative inlet profile of k based on the assumption of turbulence local equilibrium, and modified the turbulence constants in the standard k-ε turbulence model to produce an equilibrium ABL. Subsequently, Gorlé *et al.* (2009) made two turbulence model constants vary with height to ensure an equilibrium ABL when using the inlet profiles proposed by Yang *et al.* (2009). Parente *et al.* (2011) also adopted these inlet profiles, and changed the turbulence constant to be a variable. Furthermore, two source terms for the transport equations and a novel wall function for rough surface were proposed in their study to ensure an equilibrium ABL. However, the assumption of turbulence local equilibrium approximately holds true only in the near-wall region of ABL, it cannot be validated in the whole ABL (Morrison 2007). On one hand, the default turbulence constants were determined from experiments for fundamental turbulent shear flows including homogeneous shear flow and decaying isotropic grid turbulence, which have been widely used in the wall-bounded and free shear flows (Launder and Spalding 1972). On the other hand, these turbulence constants interact each other and one constant should not be changed independently, i.e., modifying one constant may improve flow behavior in one area, but may degrade it in another one (Richards and Norris 2011). Therefore, modifying the turbulence constants may not be a complete method to solve the problem.

Although many methods have been proposed to model an equilibrium ABL, it should be noted that the overwhelming majority of the existing methods use the k-ε turbulence model, and it is

recognized that this turbulence model may not perform well when a flow separation or even an adverse pressure is present (Loureiro *et al*. 2008, EI-Behery and Hamed 2011). However, the SST *k-ω* turbulence model (Menter 1994) can effectively combine the robust and accurate formulation of the standard *k-ω* turbulence model in the near-wall region with the free-stream independence of the standard *k-ε* turbulence model in the far field, by incorporating a damped cross-diffusion derivative term in the transport equations and considering the transport of the turbulence shear stress. These features make the SST *k-ω* turbulence model more accurate and reliable to predict adverse pressure gradient flows. As a result, the SST *k-ω* turbulence model has been more and more widely used in the numerical simulation of flow around bluff bodies (Yang *et al*. 2008).

However, at present, there have been few studies on modeling an equilibrium ABL based on the SST *k-ω* turbulence model with alternative inlet profiles for the turbulence properties but without modifying the turbulence constants.

Aiming at resolving these problems discussed above, to simulate an equilibrium ABL using the SST *k-ω* turbulence model in the present study, alternative inlet profiles of the mean wind speed *U* and turbulence kinetic energy *k*, were first determined. Then, the specific dissipation rate *ω* profile based on the constant shear stress condition was deduced and the source terms for *U*, *k* and *ω* according to their satisfied transport equations were derived. Finally, the equilibrium ABL in an empty computational domain was achieved by adding the above inlet profiles of *U*, *k* and *ω* and the source terms to the *k* and *ω* transport equation. Furthermore, an actual numerical simulation with a trapezoidal hill was carried out, and the numerical results with and without considering the source terms were both compared with the corresponding wind tunnel test results.

2. Modeling the equilibrium ABL using the SST *k–ω* turbulence model

2.1 SST k–ω turbulence model

The SST *k–ω* turbulence model was developed by Menter (1994), and the governing equations of the flow field including continuity equation, momentum equations, and transport equations of *k* and *ω* can be written as follows

$$\frac{\partial \rho}{\partial t} + \frac{\partial}{\partial x_i}\left(\rho u_i\right) = 0 \tag{1}$$

$$\frac{\partial}{\partial t}(\rho u_i) + \frac{\partial}{\partial x_j}\left(\rho u_i u_j\right) = -\frac{\partial p}{\partial x_i} + \frac{\partial}{\partial x_j}\left(\Gamma_U \frac{\partial u_i}{\partial x_j}\right) + S_U \tag{2}$$

$$\frac{\partial}{\partial t}(\rho k) + \frac{\partial}{\partial x_j}\left(\rho k u_j\right) = \frac{\partial}{\partial x_j}\left(\Gamma_k \frac{\partial k}{\partial x_j}\right) + \tilde{G}_k - Y_k + S_k \tag{3}$$

$$\frac{\partial}{\partial t}(\rho \omega) + \frac{\partial}{\partial x_j}\left(\rho \omega u_j\right) = \frac{\partial}{\partial x_j}\left(\Gamma_\omega \frac{\partial \omega}{\partial x_j}\right) + G_\omega - Y_\omega + D_\omega + S_\omega \tag{4}$$

where ρ is the fluid density, p is the mean pressure, Γ_U, Γ_k and Γ_ω are the effective diffusivities of

the mean fluid speed U (V or W), turbulence kinetic energy k, and specific dissipation rate ω, respectively, which are expressed as

$$\Gamma_U = \mu + \mu_t \tag{5}$$

$$\Gamma_k = \mu + \frac{\mu_t}{\sigma_k} \tag{6}$$

$$\Gamma_\omega = \mu + \frac{\mu_t}{\sigma_\omega} \tag{7}$$

and μ_t is the turbulent viscosity, which is defined as follows

$$\mu_t = \frac{\rho k}{\omega} \frac{1}{\max\left[\frac{1}{\alpha^*}, \frac{SF_2}{\alpha_1 \omega}\right]} \tag{8}$$

where σ_k and σ_ω are the turbulent Prandtl numbers for k and ω, α^* and α_1 are the model coefficient and model constant, F_2 is the blending function, and S is the modulus of the mean rate-of-strain tensor, which is given by

$$S = \sqrt{\frac{1}{2}\left(\frac{\partial u_j}{\partial u_i} + \frac{\partial u_i}{\partial u_j}\right)\left(\frac{\partial u_j}{\partial u_i} + \frac{\partial u_i}{\partial u_j}\right)} \tag{9}$$

In Eqs. (2), (3) and (4), the terms S_U, S_k, and S_ω are user-defined source terms for transport equations of U (V or W), k, and ω, respectively, $\widetilde{G}_k$ and G_ω represent the generation of k and ω, respectively, Y_k and Y_ω represent the dissipation of k and ω due to turbulence, respectively, and D_ω represents the cross-diffusion term, and they are defined as follows

$$\widetilde{G}_k = \min(\mu_t S^2, 10\rho\beta^* k\omega) \tag{10}$$

$$G_\omega = \frac{\alpha_\infty}{\nu_t} G_k = \alpha_\infty \rho S^2 \tag{11}$$

$$Y_k = \rho\beta^* k\omega \tag{12}$$

$$Y_\omega = \rho\beta_i \omega^2 \tag{13}$$

$$D_\omega = 2(1 - F_1)\rho\sigma_{\omega,2}\frac{1}{\omega}\frac{\partial k}{\partial x_j}\frac{\partial \omega}{\partial x_j} \tag{14}$$

where α_∞, β^* and β_i are the model coefficients, $\sigma_{\omega,2}$ is the model constant, and F_1 is the blending

function.

To facilitate modeling the equilibrium ABL using the SST *k-ω* turbulence model, the steady incompressible 2D flow is used in the present study, and the following conditions according to the research of Richards and Hoxey (1993) should be satisfied:

(i) The vertical speed is zero

(ii) The pressure is constant

(iii) The shear stress is constant

(iv) The turbulence kinetic energy and its specific dissipation rate satisfy their respective transport equations.

Because Eq. (1) can automatically satisfy these conditions, and in highly turbulent flows, $\mu_t \gg \mu$, the other governing Eqs. (2)-(4) can be reduced to

$$\frac{\partial}{\partial z}\left(\mu_t \frac{\partial U}{\partial z} \right) + S_U = 0 \tag{15}$$

$$\frac{\partial}{\partial z}\left(\frac{\mu_t}{\sigma_k} \frac{\partial k}{\partial z} \right) + \tilde{G}_k - Y_k + S_k = 0 \tag{16}$$

$$\frac{\partial}{\partial z}\left(\frac{\mu_t}{\sigma_\omega} \frac{\partial \omega}{\partial z} \right) + G_\omega - Y_\omega + D_\omega + S_\omega = 0 \tag{17}$$

and Eq. (9) can be reduced to

$$S = \frac{\partial U}{\partial z} \tag{18}$$

2.2 Inlet profiles of mean wind speed and turbulence properties

Generally speaking, the ABL could be divided into three parts. The lowest part is the laminar bottom layer, which could be neglected in most cases. Above the laminar bottom layer is known as the Prandtl or Surface layer where the turbulence is fully developed, and its vertical extent may reach about 200 m, depending on the thermal stratifications of the air. Above the Prandtl layer is called Ekman layer, of which height depends on the stability of the air, Coriolis parameter, etc. Above the Ekman layer is the free atmosphere, where the wind is approximately Geostrophic. From the perspectives of practical applications and further research studies, in the present study, a simplified ABL without division and in a neutral stratification is considered. Note that the lower part of the ABL (approximately in the range of Prandtl or surface layer) is the main region of human activities, where the shear stress could be treated as constant and being equal to the wall shear stress, and the mean wind speed profile can be described by a logarithmic law (Simiu and Scanlan 1996, Richards and Hoxey 1993)

$$U(z) = \frac{u_*}{\kappa} \ln\left(\frac{z + z_0}{z_0} \right) \tag{19}$$

where u_* is the friction velocity, κ is the von Kármán constant, and z_0 is the ABL aerodynamic

roughness length.

Table 1 Several main forms of k profile

Case numbers	Forms of k profile	Related references
Case 1	$k = \dfrac{u_*^2}{\sqrt{C_\mu}} = const$	Maurizi *et al.* (1998), Hargreaves and Wright (2007), Richards and Norris (2011)
Case 2	$k = \sqrt{C_1 \cdot \ln\left(\dfrac{z + z_0}{z_0}\right) + C_2}$	Yang *et al.* (2009), Gorlé *et al.* (2009)
Case 3	$k = 0.5\left(I_u(z) \cdot U(z)\right)^2$	Blocken *et al.* (2007a)
Case 4	$k = 1.0\left(I_u(z) \cdot U(z)\right)^2$	Ramponi and Blocken (2012)
Case 5	$k = 1.2\left(I_u(z) \cdot U(z)\right)^2$	Lakehal (1998)
Case 6	$k = 1.5\left(I_u(z) \cdot U(z)\right)^2$	Gao and Chow (2005)

For the inlet profiles of turbulence properties, the turbulence kinetic energy k and specific dissipation rate ω are the parameters when using the SST k-ω turbulence model. For the inlet profile of k, it does not have a unified form, and several main forms of k profile are summarized in Table 1. Some studies use a constant k profile, such as Case 1, while some studies use an alternative k profile under the assumption of turbulence local equilibrium, such as Case 2. As discussed above, the assumption of turbulence local equilibrium approximately holds true only in the near-wall region of ABL, and a drawback of this profile is that it probably has imaginary values of k at higher heights. From the perspective of the definition of k, determining its value needs the information about the standard deviations (σ) of the turbulent fluctuations in the three directions

$$k(z) = \frac{1}{2}\left(\sigma_u^2(z) + \sigma_v^2(z) + \sigma_w^2(z)\right) \tag{20}$$

However, only $\sigma_u^2(z)$ is often measured in the test, which is related to the longitudinal turbulence intensity: $I_u = \sigma_u/U$. For the other two components, different assumptions can be made, and therefore different values of $k(z)$ can be obtained (Ramponi and Blocken 2012)

(1) If $\sigma_u^2 \gg \sigma_v^2(z) \approx \sigma_w^2(z)$, it yields

$$k(z) = \frac{1}{2}\left(I_u(z)U(z)\right)^2 \tag{21}$$

(2) If $\sigma_u^2 \approx \sigma_v^2(z) + \sigma_w^2(z)$, it yields

$$k(z) = \left(I_u(z)U(z)\right)^2 \tag{22}$$

(3) If $\sigma_u^2 \approx \sigma_v^2(z) \approx \sigma_w^2(z)$, it yields

$$k(z) = \frac{3}{2}\left(I_u(z)U(z)\right)^2 \tag{23}$$

In general, the profile of $k(z)$ can be given by

$$k(z) = a\left(I_u(z)U(z)\right)^2 \tag{24}$$

where the value of a ranges from 0.5 to 1.5, and some different values of a used by different studies are summarized in Table 1, such as cases 3-6. Considering that the profile of k has a positive value throughout the ABL and normally contains the variable U (exactly U^2) (Eq. (24)), as well as considering Eq. (19), the profile of k for the SST k-ω turbulence model can be approximately expressed as

$$k(z) = u_*^2\left[C_{u1} \cdot \ln\left(\frac{z+z_0}{z_0}\right) + C_{u2}\right]^2 \tag{25}$$

where $C_{\mu1}$ and $C_{\mu2}$ are two constants that can be determined by nonlinearly fitting the Eq. (25) to the measured profile of k.

Similary, there are few studies on the profile of ω. However, if one follows the third condition "The shear stress is constant" discussed earlier, the shear stress τ will be

$$\tau = \mu_t \frac{\partial U}{\partial z} = \tau_w = \rho u_*^2 \tag{26}$$

where τ_w is the wall shear stress. Moreover, in Eq. (8), the factor $1/\max[1/\alpha*, SF_2/(\alpha_1\omega)]$ in the definition of μ_t is very complex, which will greatly increase the difficulties to compute the value of μ_t. In order to be more convenient for further studies, such as the derivation of some equations, the definition of μ_t could be simplified. Note the fact that the μ_t in the standard k-ω turbulence model (Wilcox 1998) is computed as follows

$$\mu_t = \alpha^* \frac{\rho k}{\omega} \tag{27}$$

and in highly turbulent flows, $\alpha^* = 1$. Therefore, based on the above considerations and Eq. (27), the simplified μ_t (denoted by $\tilde{\mu}_t$) could be suggested as follows

$$\tilde{\mu}_t = \rho \frac{k}{\omega} \tag{28}$$

Hereafter, μ_t is computed by using Eq. (28) instead of Eq. (8). Substituting Eqs. (19) and (28) into Eq. (26) yields the following relation

$$\frac{k}{\omega} = \kappa u_*\left(z + z_0\right) \tag{29}$$

Similarly, substituting Eq. (25) into Eq. (29) yields the following form of ω

$$\omega(z) = \frac{u_*}{\kappa(z + z_0)} \left[C_{u1} \cdot \ln\left(\frac{z + z_0}{z_0}\right) + C_{u2} \right]^2 \tag{30}$$

and hence the inlet profiles of U, k and ω are all determined via Eqs. (19), (25) and (30), respectively.

2.3 Derivation of source terms for U, k and ω transport equations

Achieving an equilibrium ABL must ensure that the inlet profiles of the mean wind speed U and turbulence properties k and ω are consistent with the turbulence model. Specifically, the fourth condition mentioned above: "The turbulence kinetic energy and its specific dissipation rate satisfy their respective transport equations" must be followed with the above determined inlet profiles. Unfortunately, neither k nor ω transport equation (Eqs. (16) and (17)) automatically satisfies this condition. In this study, the source terms S_U, S_k, S_ω are added to force the inlet profiles of U, k and ω to satisfy their respective transport equations (Eqs. (15)-(17)).

Note that the shear stress τ in Eq. (26) is a constant, substituting Eq. (26) into Eq. (15) reveals the following relation for S_U

$$S_U = 0 \tag{31}$$

Similarly, substituting Eqs. (25), (28) and (29) into the first term on the left hand side of Eq. (16) yields

$$\frac{\partial}{\partial z}\left(\frac{\mu_t}{\sigma_k}\frac{\partial k}{\partial z}\right) = \frac{2\kappa C_{u1}^2}{\sigma_k} \cdot \frac{\rho u_*^3}{(z + z_0)} \tag{32}$$

and substituting Eqs. (12), (25) and (30) into the third term on the left hand side of Eq. (16) yields

$$Y_k = \rho\beta^* k\omega = \frac{\beta^*}{\kappa} \cdot \frac{\rho u_*^3}{(z + z_0)} \left[C_{u1} \cdot \ln\left(\frac{z + z_0}{z_0}\right) + C_{u2} \right]^4 \tag{33}$$

For the second term on the left hand side of Eq. (16): $\tilde{G}_k = \min(\mu_t S^2, 10\rho\beta^* k\omega)$ (Eq. (10)), its value is equal to $\mu_t S^2$ or $10\rho\beta^*\omega$, which cannot be determined directly. Substituting Eqs. (18), (28) and (29) into Eq. (10) leads to

$$\mu_t S^2 = \frac{1}{\kappa} \cdot \frac{\rho u_*^3}{(z + z_0)} \tag{34}$$

Obviously, the form of Eq. (34) is similar to that of Eq. (32), and the term $10\rho\beta^* k\omega$ in Eq. (10) is also similar to Eq. (33) in the form. Therefore, Eq. (10) can be merged into Eqs. (32) and (33) when they add or subtract each other. Considering that Eq. (16) is satisfied, the relation for S_k can be derived as follows

$$S_k = Y_k - \frac{\partial}{\partial z}\left(\frac{\mu_t}{\sigma_k}\frac{\partial k}{\partial z}\right) - \tilde{G}_k$$

$$= \frac{\rho u_*^3}{(z+z_0)}\left\{\frac{\beta^*}{\kappa}\cdot\left[C_{u1}\cdot\ln\left(\frac{z+z_0}{z_0}\right)+C_{u2}\right]^4 - \frac{2\kappa C_{u1}^2}{\sigma_k} - \min\left(\frac{1}{\kappa},\frac{10\beta^*}{\kappa}\cdot\left[C_{u1}\cdot\ln\left(\frac{z+z_0}{z_0}\right)+C_{u2}\right]^4\right)\right\}$$

(35)

and the simplified form of S_k is

$$S_k = \frac{\rho u_*^3}{(z+z_0)}\left\{C_{1k}\cdot\left[C_{u1}\cdot\ln\left(\frac{z+z_0}{z_0}\right)+C_{u2}\right]^4 - C_{2k}\right\}$$

(36)

where C_{1k} and C_{2k} are coefficients that are newly introduced to comprehensively consider the factors β^*/κ, $10\beta^*/\kappa$, $2\kappa C_{u1}^2/\sigma_k$, and $1/\kappa$, which can simplify the form of S_k to a great degree.

The form of S_ω can be derived in a similar way. Substituting Eqs. (28)-(30) into the first term on the left hand side of Eq. (17) yields

$$\frac{\partial}{\partial z}\left(\frac{\mu_t}{\sigma_\omega}\frac{\partial\omega}{\partial z}\right) = \frac{1}{\sigma_\omega}\cdot\frac{\rho u_*^2}{(z+z_0)^2}\left\{\left[C_{u1}\cdot\ln\left(\frac{z+z_0}{z_0}\right)+C_{u2}\right]^2 - 4C_{u1}\cdot\left[C_{u1}\cdot\ln\left(\frac{z+z_0}{z_0}\right)+C_{u2}\right]+2C_{u1}^2\right\}$$

(37)

Similarly, substituting Eqs. (11) and (18) into the second term on the left hand side of Eq. (17) yields

$$G_\omega = \alpha_\infty\rho S^2 = \frac{\alpha_\infty}{\kappa^2}\cdot\frac{\rho u_*^2}{(z+z_0)^2}$$

(38)

Substituting Eqs. (13) and (30) into the third term on the left hand side of Eq. (17) yields

$$Y_\omega = \rho\beta_i\omega^2 = \frac{\beta_i}{\kappa^2}\cdot\frac{\rho u_*^2}{(z+z_0)^2}\left[C_{u1}\cdot\ln\left(\frac{z+z_0}{z_0}\right)+C_{u2}\right]^4$$

(39)

and substituting Eqs. (14), (25) and (30) into the fourth term on the left hand side of Eq. (17) yields

$$D_\omega = 2(1-F_1)\rho\sigma_{\omega,2}\frac{1}{\omega}\frac{\partial k}{\partial z}\frac{\partial\omega}{\partial z}$$

$$= 4(1-F_1)\sigma_{\omega,2}C_{u1}\cdot\frac{\rho u_*^2}{(z+z_0)^2}\cdot\left\{-\left[C_{u1}\cdot\ln\left(\frac{z+z_0}{z_0}\right)+C_{u2}\right]+2C_{u1}\right\}$$

(40)

Considering that Eq. (17) is satisfied, the relation for S_ω can be derived as follows

$$S_\omega = Y_\omega - \frac{\partial}{\partial z}\left(\frac{\mu_t}{\sigma_\omega}\frac{\partial \omega}{\partial z}\right) - G_\omega - D_\omega$$

$$= \frac{\rho u_*^2}{(z+z_0)^2}\left\{\frac{\beta_i}{\kappa^2}\cdot\left[C_{u1}\cdot\ln\left(\frac{z+z_0}{z_0}\right)+C_{u2}\right]^4 - \frac{1}{\sigma_\omega}\cdot\left[C_{u1}\cdot\ln\left(\frac{z+z_0}{z_0}\right)+C_{u2}\right]^2\right.$$

$$\left.+\left[\frac{4C_{u1}}{\sigma_\omega}+4(1-F_1)\sigma_{\omega,2}C_{u1}\right]\cdot\left[C_{u1}\cdot\ln\left(\frac{z+z_0}{z_0}\right)+C_{u2}\right]-\left[\frac{2C_{u1}^2}{\sigma_\omega}+\frac{\alpha_\infty}{\kappa^2}+8(1-F_1)\sigma_{\omega,2}C_{u1}^2\right]\right\} \tag{41}$$

and the form of S_ω can be further simplified as

$$S_\omega = \frac{\rho u_*^2}{(z+z_0)^2}\left\{C_{1\omega}\cdot\left[C_{u1}\cdot\ln\left(\frac{z+z_0}{z_0}\right)+C_{u2}\right]^4 - C_{2\omega}\cdot\left[C_{u1}\cdot\ln\left(\frac{z+z_0}{z_0}\right)+C_{u2}\right]^2\right.$$

$$\left.+C_{3\omega}\cdot\left[C_{u1}\cdot\ln\left(\frac{z+z_0}{z_0}\right)+C_{u2}\right]-C_{4\omega}\right\} \tag{42}$$

where $C_{1\omega}$, $C_{2\omega}$, $C_{3\omega}$ and $C_{4\omega}$ are coefficients, which are also newly introduced to comprehensively consider the corresponding term in the original Eq. (41).

Therefore, the simplified forms of the source terms S_U, S_k and S_ω are all derived via Eqs. (31), (36) and (42), respectively. However, how to determine the forms of these six coefficients C_{1k}, C_{2k}, $C_{1\omega}$, $C_{2\omega}$, $C_{3\omega}$ and $C_{4\omega}$ remain to be an issue. On one hand, since the source terms S_k and S_ω are obtained based on the "simplified" turbulent viscosity $\tilde{\mu}_t$ (Eq. (28)), the exact coefficients in Eqs. (35) and (41) should be more complex than presented; on the other hand, the definitions of many coefficients in the SST k-ω turbulence model are also complex, such as α_∞, β_i, β^*, etc. (Fluent Inc. 2006). Therefore, the exact forms of the above six coefficients in Eqs. (36) and (42) are probably too complicated to obtain easily. To be more convenient for the practical applications and to weaken the influences of $\tilde{\mu}_t$ and the complex model coefficients on the forms of the six new coefficients, a reasonable treatment is to assume these six coefficients being constants. Although determining the values of these constant coefficients is still difficulty, it can be seen from Eq. (41) that the first term (in brace) is positive, the second and fourth terms are negative, while the sign of the third term is related to the values of $C_{\mu1}$ and $C_{\mu2}$. Consider that the second and fourth terms have a similar effect on the flow field, so does the first and third terms if the third term is also positive. Since the terms in the specific dissipation rate ω (or dissipation rate ε for the k-ε turbulence model) transport equation are commonly assumed to have similar mechanisms and forms with the corresponding terms in the turbulence kinetic energy k transport equation in modeling a turbulence enclosure model (Fluent Inc. 2006), in other words, the following relation should be satisfied

$$f(\omega) = C_\omega \cdot \frac{\omega}{k} \cdot f(k) \tag{43}$$

where $f(k)$ and $f(\omega)$ are the corresponding terms in the k and ω transport equation, respectively, such as dispersion, generation and dissipation terms, etc., and C_ω is a coefficient. The ω related

terms in Eq. (43) are changed to the corresponding ε terms for the k-ε turbulence model.

If the relationship by Eq. (43) is also applicable to Eqs. (35) and (41), it is not hard to find that the second and third terms in Eqs. (41) and (42) will not exist. According to the above analysis and assume that the effects of the second and third terms in Eq. (41) on the flow field can be represented by the other two terms, the coefficients $C_{2\omega}$ and $C_{3\omega}$ in Eq. (42) can thus be determined to be zero, which also can simplify the form of S_ω. For the other four coefficients C_{1k}, C_{2k}, $C_{1\omega}$ and $C_{4\omega}$, some trial case studies showed that the coefficients C_{1k} and $C_{1\omega}$ are more sensitive to the horizontal homogeneity of the flow field than the coefficients C_{2k} and $C_{4\omega}$. Therefore, firstly the values of coefficients C_{1k} and $C_{1\omega}$, then the values of coefficients C_{2k} and $C_{4\omega}$ could be roughly determined, and lastly, a minor adjustment for the four coefficients should be made together to obtain an appropriate set of coefficients for ensuring an equilibrium ABL.

3. Validation of the equilibrium ABL and its effects on the wind field above a hill

To validate the effectiveness of the above inlet profiles of U, k and ω and with the source terms S_k and S_ω being added to the k and ω transport equations respectively for modeling an equilibrium ABL, a numerical case study based on a wind tunnel test (Shiau and Hsu 2003) is carried out in an empty computational domain. Furthermore, an actual simulation with a trapezoidal hill is conducted, and the numerical results with and without considering the source terms are compared with the corresponding wind tunnel test results, respectively.

3.1 Wind tunnel test and numerical model description

The tests were conducted in the 2.0 m-wide, 1.4 m-high and 12.5-long test section of an open suction wind tunnel by Shiau and Hsu (2003). A 2D trapezoidal shape of hill model of height H = 0.05m with the smooth surface was adopted, and the schematic diagram of the hill model is shown in Fig. 1. In this test, a rural terrain type of neutral ABL was simulated with a model/field scale of 1/300. The measured mean wind speed profile is shown in Fig. 2(a), where the power exponent is about 0.16 if the mean wind speed profile is described by the power law. This value is in the range of 0.143-0.167 as proposed by Counihan (1975) for the rural terrain type of neutral ABL flow. Moreover, the simulated longitudinal and vertical turbulence intensity profiles are shown in Fig. 2(b). It can be seen from the figure that the simulated longitudinal turbulence intensity close to the wall is about 15%. Counihan (1975) had found that the longitudinal turbulence intensity close to the ground in the rural terrain areas is in the range of 10–20%. For more details, refer to Shiau and Hsu (2003).
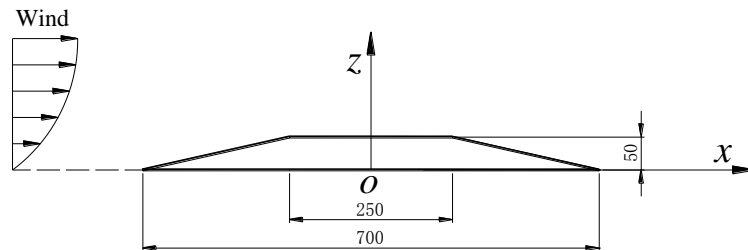

Fig. 1 Schematic diagram of the trapezoidal hill model and the coordinate system (dimensions are given in mm)

Before the numerical simulation, the inlet profiles of U, k and ω should be determined first. For the U profile, it can be directly fitted to the logarithmic law (Eq. (19)) from Fig. 2(a). However, the k profile cannot be directly determined from Fig. 2(b) based on the Eq.(24). On the one hand, the relationship $I_u > I_v > I_w$ always holds in the ABL; on the other hand, the average value of I_w/I_u in Fig. 2(b) equals to about 0.73. Therefore, the value of a in Eq. (24) ranges from 1.0-1.5 for the present wind tunnel test. For convenience, the value of a is assumed to be equal to the middle value of this range, i.e., $a = 1.25$ in this study. Then, the ω profile can be determined by Eq.(30).

According to the setups of the wind tunnel test, firstly, a 2D empty computational domain with 6.0 m in the longitudinal direction (x) and 1.4 m in the vertical direction (z) is adopted. The computational domain is discretized by a structured grid, and the finer grid is used at the position where the hill model is located (The hill model is located at the 1/3 of the total length in the longitudinal direction). The height from the center of the wall-adjacent cell to the bottom wall is 0.0025 m. As a result, the total number of cells is 13,200. In this investigation, the CFD commercial software FLUENT 6.3 is employed, and the flow is supposed to be incompressible and steady. The boundary conditions for the numerical model with the SST k-ω turbulence model are listed in Table 2, in which the inlet boundary adopts the inlet profiles of U, k and ω presented by Eqs. (19), (25) and (30), respectively, and the values of some parameters in the U profile and coefficients in the k profile are determined through nonlinearly fitting the wind tunnel test data.

They are u_*=0.447 m/s, κ=0.41, z_0=2.0×10^{-4} m, $C_{\mu 1}$=-0.422, and $C_{\mu 2}$=4.568. Fig. 3 shows the fitted inlet profiles of U and k comparing with the corresponding values based on the wind tunnel test data. It can be seen that the fitting accuracy is high. At the bottom of the computational domain, a rough wall is modeled, and the corresponding parameters, the roughness height K_s=0.00245 m and roughness constant C_s=0.8 are determined by the requirement of Blocken *et al.* (2007b). The top of the computational domain are modeled as symmetry boundary condition, and at the outlet, the pressure- outlet boundary condition is applied. When choosing the discretization schemes for the governing equations, the SIMPLEC algorithm is applied to the pressure-velocity coupling, the second order interpolation scheme is used for pressure, and the second order upwind scheme is adopted for moment and turbulence properties. The values set for the inlet boundary are used to initialize the flow field, and the scaled residuals for all variables are set to be 10^{-6}.
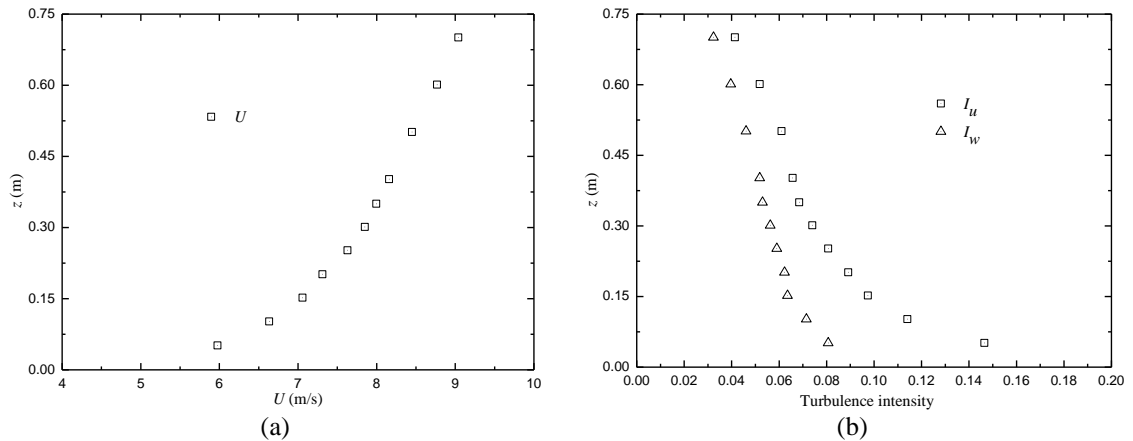

Fig. 2 Measured wind speed profile and turbulence intensity profiles: (a) Wind speed profile and (b) Longitudinal and vertical turbulence intensity profiles
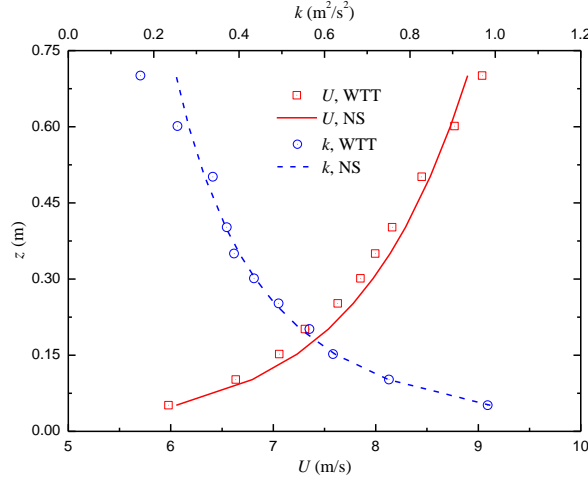
Fig. 3 Fitted inlet profiles of U and k compared with the corresponding values based on wind tunnel test data. For two cases: WTT refers to the values based on the wind tunnel test (Shiau and Hsu 2003), NS refers to the fitted inlet profiles used for the numerical simulation

Table2 Boundary conditions and parameters in U, k and ω profiles

Boundaries		Boundary conditions and Parameters
Inlet	Velocity inlet	$U(z) = \dfrac{0.447}{0.41}\ln\left(\dfrac{z+0.0002}{0.0002}\right),\ \ v=0,\ \ w=0$ $k(z) = 0.447^2\left[-0.422\cdot\ln\left(\dfrac{z+0.0002}{0.0002}\right)+4.568\right]^2$ $\omega(z) = \dfrac{0.447}{0.41\cdot(z+0.0002)}\left[-0.422\cdot\ln\left(\dfrac{z+0.0002}{0.0002}\right)+4.568\right]^2$
Outlet	Pressure-outlet	$p=0$
Top	Symmetry	$w=0,\ \dfrac{\partial(U,v,k,\omega)}{\partial z}=0$
Bottom	Wall	Roughness height K_s=0.00245m and roughness constant C_s=0.8.

3.2 Validation of the equilibrium ABL

As mention earlier, an equilibrium ABL should be achieved in an empty computational domain before the actual CFD simulation. Based on the above determined inlet profiles of U, k and ω, to investigate the effects of the source terms S_k and S_ω presented by Eqs. (36) and (42) on the flow field, the performance of U, k and ω profiles along the empty computational domain with and without adding the source terms to the k and ω transport equations (Eqs. (16) and (17)) are comparatively studied. When considering the two source terms S_k and S_ω, the values of coefficients C_{1k}, C_{2k}, $C_{1\omega}$ and $C_{4\omega}$ ($C_{2\omega}$=$C_{3\omega}$=0) can be determined by the approach introduced at the end of the

section 2.3. The source terms and the corresponding coefficients are shown in Table 3.

For the results without considering the source terms, the inlet profiles, the incident profiles (defined as those that would occur at the hill model position) and the outlet profiles are shown in
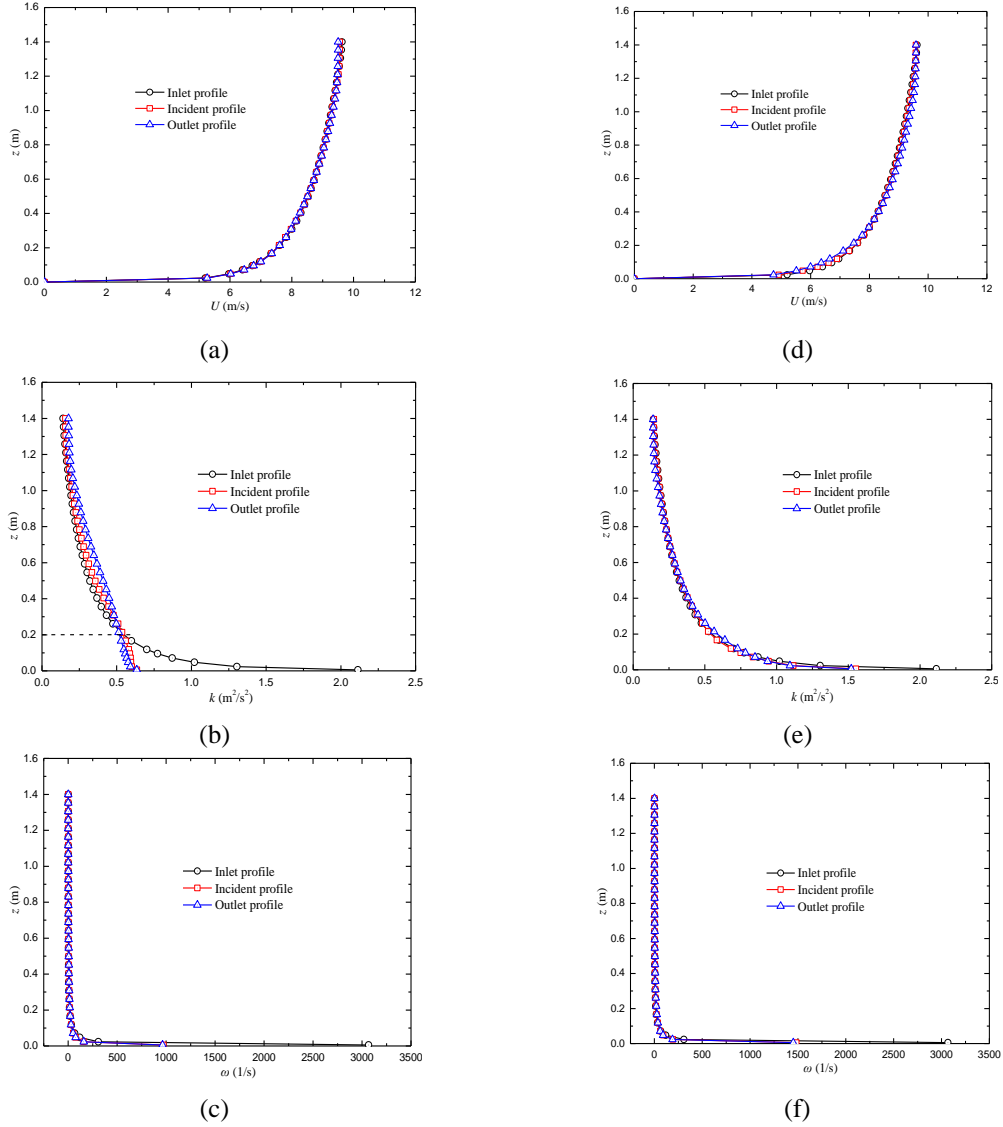

(a)   (d)

(b)   (e)

(c)   (f)

Without considering the source terms S_k and S_ω With considering the source terms S_k and S_ω

Fig. 4 Comparison of U, k and ω profiles at different positions along the empty computational domain with and without considering the source terms S_k and S_ω: (a) U profiles, (b) k profiles and (c) ω profiles at different positions without considering source terms; (d) U profiles, (e) k profiles and (f) ω profiles at different positions with considering source terms

Figs. 4(a)-4(c). Although the profiles of U and ω could be approximately maintained throughout the computational domain, the profiles of k have a great difference between the inlet profile and the incident profile (or the outlet profile), especially for the heights smaller than 0.2 m, which implies that there exists a significant gradient along the domain. Therefore, the equilibrium ABL is not obtained when the source terms are not considered. However, the profiles of U, k and ω with considering the source terms are all maintained well throughout the domain, as shown in Figs. 4(d)-4(f), which indicates that an equilibrium ABL is satisfactorily achieved when the source terms are considered. It should be noted that the biggest difference between the Figs. 4(a)-4(c) and Fig. 4(d)-4(f) is the profiles of k, and the average relative error (comparisons of inlet profiles and incident profiles) in Fig. 4(b) reaches to 13.9%, but the average relative error in Fig. 4(e) is only 2.5%. In summary, through the comparative results with and without considering the sources terms, the inlet profiles of U, k and ω, with the source terms S_k and S_ω being added to the k and ω transport equations, respectively, can effectively achieve an equilibrium ABL.

Table3 Source terms for k and ω transport equations and related coefficients

Transport equations	Source terms and coefficients
k transport equation	$S_k = \dfrac{1.225 \times 0.447^3}{(z+0.0002)}\left\{0.054\cdot\left[-0.422\cdot\ln\left(\dfrac{z+0.0002}{0.0002}\right)+4.568\right]^4 - 0.805\right\}$
ω transport equation	$S_\omega = \dfrac{1.225 \times 0.447^2}{(z+0.0002)^2}\left\{0.006\cdot\left[-0.422\cdot\ln\left(\dfrac{z+0.0002}{0.0002}\right)+4.568\right]^4 - 0.215\right\}$

3.3 Effects of equilibrium ABL on the wind field above a hill

To investigate the effects of the proposed inlet profiles of U, k and ω and source terms S_k and S_ω on achieving an equilibrium ABL for practical applications, an actual numerical simulation with a trapezoidal hill (shown in Fig. 1) is conducted, as described earlier. Here, the numerical results with and without considering the source terms are both compared with the corresponding wind tunnel test results (Shiau and Hsu 2003).

The profiles of mean wind speed ratio $U/U_{z=1.0}$ ($U_{z=1.0}$ is defined as the mean wind speed of height $z=1.0$ m at the inlet boundary) and turbulence intensity at the position $x=0.0$m (shown in Fig. 1) are shown in Figs. 5(a) and 5(b). The two profiles of mean wind speed ratios obtained by numerical simulation are both close to the wind tunnel test results and the average relative error is only about 2.2%. The numerical results of the turbulence intensity profile with considering the source terms acceptably agree with the wind tunnel test results; while the numerical results of the turbulence intensity profile without considering the source terms can be generally divided into two parts: for the part that the heights are larger than 0.2 m, the numerical results have also an acceptable agreement with the wind tunnel test results. However, for the part that the heights are smaller than 0.2 m, the numerical results are significant different from the wind tunnel test results and the average relative error is about 12.9%.

It can be seen from Figs. 4(a) and 4(d) that the U profiles can be generally maintained along the

domain whether the source terms are considered or not. Therefore, the numerical results of the two mean wind speed ratio profiles shown in Fig. 5(a) are almost the same, and they both show a relatively high accuracy. However, the lower part of the k profile changes greatly along the domain when the source terms are not considered (shown in Fig. 4(b)). For this reason, the corresponding numerical results of the lower part of the turbulence intensity profile (heights are smaller than 0.2 m) has a serious error.   Note that the lower part of the wind field above a complex terrain (such as the trapezoidal hill in this study) is usually more concerned in the structural wind engineering (Cao *et al*. 2012, Yamaguchi *et al*. 2003, Kim *et al*. 2000). In summary, the equilibrium ABL directly affects the results of the actual numerical simulation, and achieving an equilibrium ABL based on the proposed inlet profiles and source terms can greatly improve the accuracy of the numerical simulation.
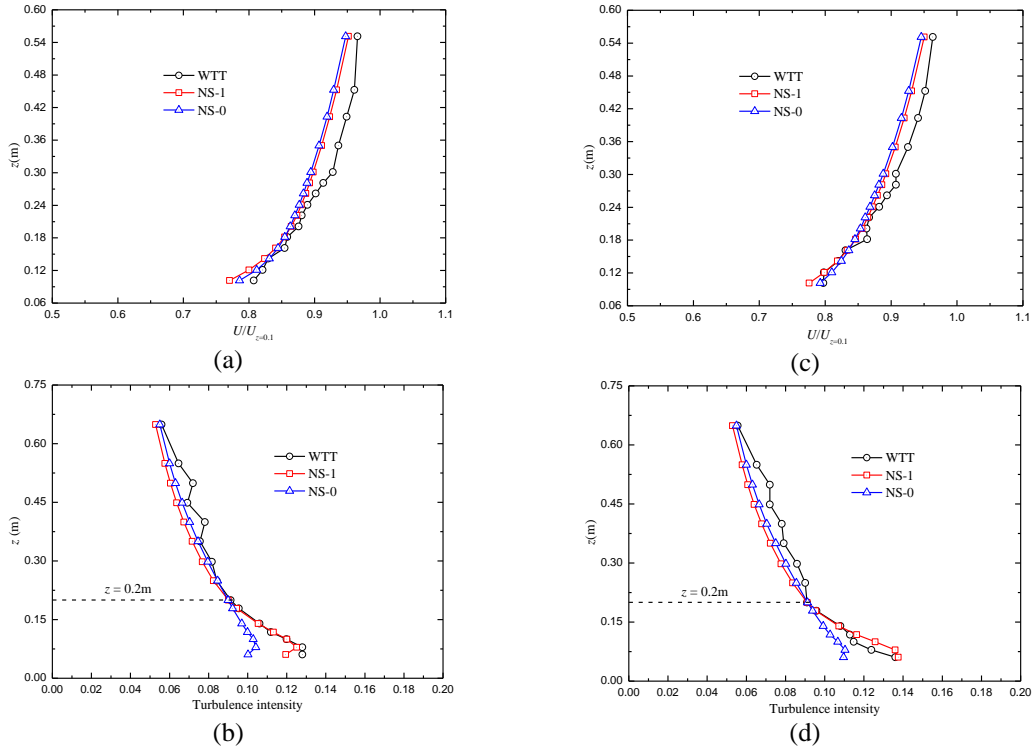

Fig. 5 Comparison of numerical results of mean wind speed ratio and turbulence intensity with the corresponding wind tunnel test results at positions x=0.0 m and x=-0.125 m: (a) Mean wind speed ratio results at x=0.0 m, (b) Turbulence intensity results at x=0.0 m, (c) Mean wind speed ratio results at x=-0.125 m and (d) Turbulence intensity results at x=-0.125 m. For three cases: WTT refers to the results obtained by the wind tunnel test (Shiau and Hsu 2003), NS-1 refers to the results obtained by numerical simulations with considering the source terms and NS-0 refers to the results obtained by numerical simulations without considering the source terms. Here the turbulence intensity is defined as the root mean square of longitudinal wind speed fluctuation normalized by the local mean wind speed of upstream position at x=-1.0 m (Shiau and Hsu 2003)

Moreover, the profiles of mean wind speed ratio $U/U_{z=1.0}$ and turbulence intensity at the upstream position $x=-0.125$ m (shown in Fig. 1) are shown in Figs. 5(c)-5(d). The variations of the mean wind speed ratio profiles (Fig. 5(c)) and turbulence intensity profiles (Fig. 5(d)) are quite similar to those in Figs. 5(a) and 5(b), respectively. Furthermore, the differences between the numerical results and the wind tunnel test results in Figs. 5(c) and 5(d) are also generally similar to those in Figs. 5(a) and 5(b), respectively. From these numerical results, it can be concluded that the proposed inlet profiles of U, k and ω and source terms S_k and S_ω to achieve an equilibrium ABL is valid for the actual simulation.

4. Conclusions

An equilibrium ABL should be achieved in an empty computational domain before the actual CFD simulation is conducted with structures. Up to now, the overwhelming majority of methods for modeling the equilibrium ABL have used the k-ε turbulence model. In this paper, based on the SST k-ω turbulence model, the equilibrium ABL is satisfactorily achieved in an empty computational domain when the proposed inlet profiles of mean wind speed U, turbulence kinetic energy k, and specific dissipation rate ω and the source terms S_k and S_ω are adopted. Furthermore, an actual simulation with a trapezoidal hill is conducted, and the comparisons of results between the numerical simulation and the wind tunnel test show that the proposed inlet profiles and source terms to achieve an equilibrium ABL can greatly improve the accuracy of the actual numerical simulation.

Although only the SST k-ω turbulence model is investigated in the present study, the developed methodology to determine the inlet profiles and source terms can also be applied to other two-equation turbulence models, such as the standard, RNG, realizable k-ε turbulence models and the standard k-ω turbulence model. While the present study has provided a new methodology for modeling the equilibrium ABL problem and for further CFD simulations with practical application value, it is also important to mention the limitations of this study:

(1) The assumption of constant shear stress and the mean wind speed profile described by Eq. (19) are valid only in the Prandtl or surface layer, not in the entire ABL.

(2) The study was only performed for the rural terrain type and did not investigate the other types of terrains.

(3) The study was only performed for the neutral ABL and did not investigate the stable and unstable stratification.

These limitations will be focused on in the future study.

Acknowledgements

References

Blocken, B., Carmeliet, J. and Stathopoulos, T. (2007a), "CFD evaluation of wind speed conditions in passages between parallel buildings-effect of wall-function roughness modifications for the atmospheric boundary layer flow", *J. Wind Eng. Ind. Aerod.*, **95** (9-11), 941-962.

Blocken, B., Janssen, W.D. and van Hooff, T. (2012), "CFD simulation for pedestrian wind comfort and wind safety in urban areas: General decision framework and case study for the Eindhoven University campus", *Environ. Modell. Softw.*, **30**, 15-34.

Blocken, B., Stathopoulos, T. and Carmeliet, J. (2007b), "CFD simulation of the atmospheric boundary layer: wall function problems", *Atmos. Environ.*, **41** (2), 238- 252.

Cao, S., Wang, T., Ge, Y. and Tamura, Y. (2012), "Numerical study on turbulent boundary layers over two-dimensional hills—Effects of surface roughness and slope", *J. Wind Eng. Ind. Aerod.*, **104-106**, 342-349.

Counihan, J. (1975), "Adiabatic atmospheric boundary layers: a review and analysis of data from the period 1880-1972", *Atmos. Environ.*, **9**(10), 871- 905.

EI-Behery, S.M. and Hamed, M.H. (2011), "A comparative study of turbulence models performance for separating flow in a planar asymmetric diffuser", *Comput. Fluids*, **44**(1), 248-257.

Fluent Inc. (2006), *Fluent 6.3 User's Guide*, Fluent Inc., Lebanon, New Hampshire.

Franke, J., Hellsten, A., Schlünzen, H. and Carissimo, B. (2007), *Best practice guideline for the CFD simulation of flows in the urban environment*, COST Office, Brussels.

Gao, Y. and Chow, W.K. (2005), "Numerical studies on air flow around a cube", *J. Wind Eng. Ind. Aerod.*, **93**(2), 115-135.

Gorlé, C., van Beeck, J., Rambaud, P. and van Tendeloo, G. (2009), "CFD modelling of small particle dispersion: the influence of the turbulence kinetic energy in the atmospheric boundary layer", *Atmos. Environ.*, **43**(3), 673-681.

Hargreaves, D.M. and Wright, N.G. (2007), "On the use of the k-ε model in commercial CFD software to model the neutral atmospheric boundary layer", *J. Wind Eng. Ind. Aerod.*, **95**(5), 355-369.

Kim, H.G., Patel, V.C. and Lee, C.M. (2000), "Numerical simulation of wind flow over hilly terrain", *J. Wind Eng. Ind. Aerod.*, **87**(1), 45-60.

Lakehal, D. (1998), "Application of the k-ε model to flow over a building placed in different roughness sublayers", *J. Wind Eng. Ind. Aerod.*, **73**(1), 59-77.

Launder, B.E. and Spalding, D.B. (1972), *Lectures in mathematical models of turbulence*. Academic Press, London, England.

Loureiro, J.B.R., Alho, A.T.P. and Silva Freire, A.P. (2008), "The numerical computation of near-wall turbulent flow over a steep hill", *J. Wind Eng. Ind. Aerod.*, **96**(5), 540-561.

Maurizi, A., Palma, J.M.L.M. and Castro, F.A. (1998), "Numerical simulation of the atmospheric flow in a mountainous region of the North of Portugal", *J. Wind Eng. Ind. Aerod.*, **74-76**, 219-228.

Menter, F.R. (1994), "Two-equation eddy-viscosity turbulence models for engineering applications", *AIAA J.*, **32**(8), 1598-1605.

Morrison, J.F. (2007), "The interaction between inner and outer regions of turbulent wall-bounded flow", *Philos. T. R. Soc. A.*, **365**, 683-698.

Parente, A., Gorlé, C., van Beeck, J. and Benocci, C. (2011),"Improved k-ε model and wall function formulation for the RANS simulation of ABL flows", *J. Wind Eng. Ind. Aerod.*, **99**(4), 267-278.

Ramponi, R. and Blocken, B. (2012), "CFD simulation of cross-ventilation for a generic isolated building: Impact of computational parameters", *Build. Environ.*, **53**, 34-48.

Richards, P.J. and Hoxey, R.P. (1993), "Appropriate boundary conditions for computational wind engineering models using the k–ε turbulence model", *J. Wind Eng. Ind. Aerod.*, **46-47**, 145-153.

Richards, P.J. and Norris, S.E. (2011), "Appropriate boundary conditions for computational wind engineering models revisited", *J. Wind Eng. Ind. Aerod.*, **99**(4), 257-266.

Riddle, A., Carruthers D., Sharpe, A., Mchugh, C. and Stocker, J. (2004), "Comparisons between FLUENT

and ADMS for atmospheric dispersion modelling", *Atmos. Environ.*, **38**(7), 1029-1038.

Shiau, B.S. and Hsu, S.C. (2003), "Measurement of the Reynolds stress structure and turbulence characteristics of the wind above a two-dimensional trapezoidal shape of hill", *J. Wind Eng. Ind. Aerod.*, **91**(10), 1237-1251.

Simiu, E. and Scanlan, R.H. (1996), *Wind effects on structures: fundamentals and applications to design,* 3rd Ed., John Wiley, New York.

Wilcox, D.C. (1998), *Turbulence modeling for CFD*. DCW Industries, La Canada, California.

Yamaguchi, A., Ishihara, T. and Fujino, Y. (2003), "Experimental study of the wind flow in a coastal region of Japan", *J. Wind Eng. Ind. Aerod.*, **91**(1-2), 247-264.

Yang, W., Quan, Y., Jin, X., Tamura, Y. and Gu, M. (2008), "Influences of equilibrium atmosphere boundary layer and turbulence parameter on wind loads of low-rise building", *J. Wind Eng. Ind. Aerod.*, **96**(10-11), 2080-2092.

Yang, Y., Gu, M., Chen, S. and Jin, X. (2009), "New inflow boundary conditions for modelling the neutral equilibrium atmospheric boundary layer in computational wind engineering", *J. Wind Eng. Ind. Aerod.*, **97**(2), 88-95.

JH